HYDROTHERMAL INTERACTION OF WYOMING BENTONITE AND OPALINUS CLAY

Kirsten Sauer[1] * , Florie Caporuscio[1], Marlena Rock[1], Michael Cheshire[2], and Carlos Jové-Colón[3]

[1]Los Alamos National Laboratory, EES-14, MS J966, P.O. Box 1663, Los Alamos, NM 87545, USA
[2]Oak Ridge National Laboratory, 1 Bethel Valley Road, Oak Ridge, TN 37831, USA
[3]Sandia National Laboratories, 1515 Eubank SE, Albuquerque, NM 87123, USA

Abstract—Most investigations into clay-mineral stability and new mineral formation within engineered barrier system (EBS) materials for geologic repositories of nuclear waste have focused on temperatures <100°C. In response to the United States Department of Energy's interest in disposing of waste packages with higher thermal loads, higher temperature (200–300°C) and pressure (~150 bar), long-term (6-week to 6-month), hydrothermal experiments were conducted to evaluate the interaction of Opalinus Clay (wall rock) and Wyoming bentonite (clay buffer) with synthetic Opalinus Clay groundwater. Experiments were conducted in autoclaves using a flexible gold reaction cell with water:rock ratios between 6:1 and 9:1. Run products were characterized in terms of mineralogy and geochemistry. Montmorillonite remained stable at 200 and 300°C; traces of illite-smectite interstratified minerals were observed. Clay minerals in Opalinus Clay experienced significant changes at 300°C, including the formation of illite, illite-smectite, and chlorite-smectite. Montmorillonite illitization within the Wyoming bentonite EBS material was likely limited by the bulk chemistry of the system (i.e. low potassium) and newly formed illite was likely limited to the Opalinus Clay fragments, nucleating on pre-existing illite in the clay rock. Zeolite minerals with compositions between analcime and wairakite formed at 300°C along edges of Opalinus Clay fragments and within the bentonite matrix, but not at 200°C. Aqueous fluids remained undersaturated with respect to quartz in Opalinus Clay ± Wyoming bentonite 300°C experiments, and dissolution and re-precipitation of phases such as kaolinite, calcite, and smectite likely contributed to zeolite formation. These results can be applied to understanding zeolite formation, clay-mineral phase stability, and silica saturation within EBS materials of a high-temperature repository.

Key Words—Analcime · High-temperature repository · Hydrothermal · Montmorillonite · Opalinus Clay · Wyoming bentonite

INTRODUCTION

The Spent Fuel and Waste Disposition program of the U.S. Department of Energy (DOE) aims to investigate the design and safety function of deep geological nuclear waste repositories in a variety of host-rock settings. Proposed repository designs vary but typically include a metal canister surrounded by bentonite backfill, and emplaced within a host rock, referred to as the engineered barrier system (EBS) (Fig. 1). Potential candidate host-rock formations for the repository include crystalline (e.g. granite), sedimentary (e.g. argillite/clay rock), and salt. This experimental study is focused on an argillite-hosted repository, and the interaction of Opalinus Clay (argillite wall rock) and Wyoming bentonite (clay barrier backfill).

The proposed components of the repository all have favorable properties for isolating radioactive material at ambient temperatures and pressures and under dry conditions. The U.S., however, is exploring disposing of spent nuclear fuel (SNF) assemblies (e.g. pressurized water reactors, PWRs) in configurations that may result in significant increases in repository temperatures. Modeling of the thermal evolution of a 32-PWR (60 gigawatt-days per metric ton burnup) SNF waste package emplaced within a shale host rock (25 year ventilation; 15 m package spacing) indicates the potential for canister surface temperatures to reach 299°C after 85 y (Greenberg et al. 2013). At these elevated temperatures and in the presence of water, irreversible mineralogical changes within the benton-

ite backfill and at the wall rock–bentonite interface will occur during peak thermal conditions.

Many studies have focused on the long-term stability of candidate geologic materials used in disposal concepts including several large-scale, multi-decade, in situ heater tests (e.g. FEBEX at the Grimsel Test Site (Martin et al. 2006) and Prototype Repository at the Äspö Hard Rock Laboratory (Johannesson et al. 2007)). Full-scale heater tests provide valuable information about post-closure physical, geochemical, and mineralogical changes in the repository system (e.g. Dohrmann et al. 2013; Dohrmann and Kaufhold 2014; Fernandez et al. 2018; Hadi et al. 2019). The completed full-scale studies to date have focused on temperatures <150°C, limiting comparison to disposal associated with a higher thermal load. Modeling studies characterize the mineralogical evolution of the repository system, but may not fully capture complex, coupled, mineral reactions in the engineered system (e.g. Zheng et al. 2015). Experimental studies, including the present study, can provide insight into key mineralogical and geochemical changes in a simplified system that can be utilized in models to understand long-term repository function and introduce hypotheses that can be tested in full-scale experiments.

The overall objective of the present study was to assess the long-term performance of engineered barrier materials in a

---

* E-mail address of corresponding author: sauer@lanl.gov
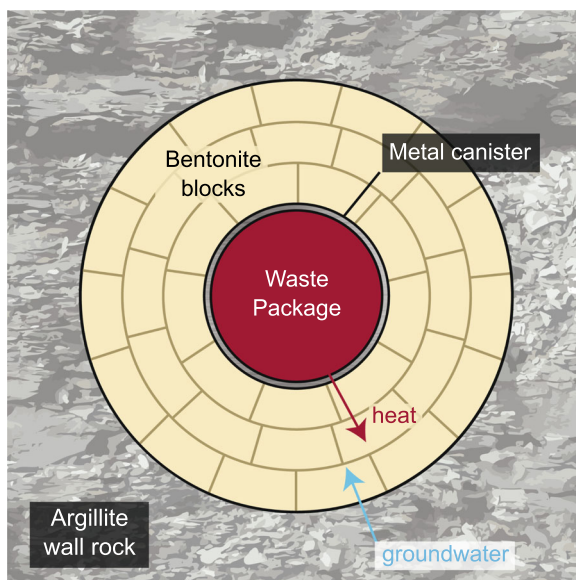
Fig. 1. Schematic of a generic engineered barrier system concept in argillite host rock. Bentonite blocks surround a waste canister emplaced in a horizontal tunnel.

high-temperature, argillite-hosted nuclear waste repository. Material transformations at temperatures of 200–300°C and pressures of 150 bar were tested in seven long-term (6-week to 6-month) hydrothermal experiments using Opalinus Clay from Mont Terri, Switzerland, and Wyoming bentonite from Colony, Wyoming. Further objectives were to select experimental conditions (e.g. fully saturated conditions) that encouraged mineral reactions to reach near steady state over the experiment duration, to characterize the reaction product mineralogy and geochemistry in order to identify clay-mineral and zeolite-forming reactions that are of concern for bentonite stability, and to uncover any links between aqueous geochemical changes and the mineral reactions.

BACKGROUND

Wyoming Bentonite

Bentonite has long been proposed as an EBS material for nuclear waste due to its availability and large clay mineral content (e.g. Pusch 1979). Clay minerals provide a chemical barrier that can attenuate radionuclide migration and a physical barrier due to the ability of expansive clay to swell, seal cracks, and preclude groundwater infiltration (Pusch 1979; Dohrmann et al. 2013; Sellin and Leupin 2014). The bentonite used in the present study was provided by Bentonite Performance Minerals LLC from Colony, Wyoming, U.S.A. and is composed dominantly of Na-montmorillonite (general composition: $Na_{0.33}(Al,Mg)_2(Si_4O_{10})(OH)_2 \cdot nH_2O$), lesser clinoptilolite and feldspar, and minor biotite, pyrite, quartz, and opal. Under dry conditions, the bentonite mineral assemblage may be stable to over 350°C (Wersin et al. 2007); however, moisture is likely to be present in the natural geologic environment. Under water-saturated conditions and temperatures >100°C, alteration of

clay minerals may occur (e.g. Mosser-Ruck et al. 2010; Ferrage et al. 2011; Cheshire et al. 2014). Both laboratory and in situ (full-scale) experiments can provide insight into the stability of bentonite at repository conditions and are, therefore, important in assessing the long-term function of a nuclear waste disposal site.

Mineralogical changes within the bentonite EBS materials that affect the ability of smectite to expand are a primary concern for the long-term function of a nuclear waste repository. The reduction of swelling capacity of smectite, due to the formation of non-swelling clays, cementation of smectite lamellae caused by silica precipitation, and/or recrystallization to other mineral phases (e.g. zeolites), is believed to be one of the greatest risks to the repository stability and isolation capability compared to other mineral reactions (Pusch et al. 1998; Pusch and Kasbohm 2002). Previous laboratory-scale investigations have investigated clay mineral transformations relevant to EBS systems over a wide range of repository temperatures (i.e. ~25 to 300°C), alone and in contact with metals that approximate potential canister materials (Madsen 1998; Meunier et al. 1998; Guillaume et al. 2003; Hofmann et al. 2004; Wersin et al. 2007; Mosser-Ruck et al. 2010; Ferrage et al. 2011; Cheshire et al. 2014).

The reduction of swelling capacity of montmorillonite may be due dominantly to the formation of non-swelling clays (e.g. illite, $K(Al,Mg,Fe)_2(Si,Al)_4O_{10}[(OH)_2]$) (Wersin et al. 2007). For example, in experimental systems where K^+ was reacted with bentonite, the formation of non-swelling K^+ rich, collapsed layer smectite and/or illite was observed (e.g. Mosser-Ruck et al. 1999; Kaufhold and Dohrmann 2010; Cheshire et al. 2014). In the alteration of montmorillonite to illite, silica is liberated through the generalized reaction:

$$Na\text{-montmorillonite} + K^+ + H^+ \rightarrow illite + SiO_{2(aq)} \quad (1)$$
$$+ Na^+ + Mg^+ + H_2O$$
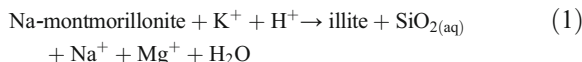
The low availability of K^+ and silica saturation in the system may limit illitization (Pusch and Madsen 1995; Cheshire et al. 2014; Savage et al. 2019). For example, in bentonite systems reacted with NaCl solutions, montmorillonite structural alteration is not observed (Kaufhold and Dohrmann 2009; Cheshire et al. 2014) in comparison to experiments in a K^+ rich environment (Kaufhold and Dohrmann 2010).

The influence of bulk chemistry on clay-mineral reactions is observed in full-scale experiments. In the full-scale Prospective Repository experiment at the Äspö Hard Rock Laboratory in Sweden, cation exchange was observed in the smectite, but no structural changes were observed in the bentonite blocks after a period of eight years at temperatures between 60 and 85°C (Dohrmann and Kaufhold 2014). In the FEBEX experiment, smectite alteration was observed only close to the heater surface (100°C) and included recrystallization to saponite and chlorite and a decrease in cation exchange capacity and surface area (Fernandez et al. 2018).

Zeolite formation within bentonite EBS material has also been reported (e.g. Mosser-Ruck et al. 2010; Ferrage et al. 2011; Cheshire et al. 2013, 2014; Mosser-Ruck et al. 2016). Zeolites may form as a result of clinoptilolite dissolution under

Table 1. Experiment run components and conditions.

Exp. No.	Synthetic groundwater (mL)	Opalinus Clay (g)	Wyoming bentonite (g)	EBS metal type	EBS metal (g)	Fe° (g)	Fe₃O₄ (g)	Deviations	Run T (°C)	Run time	Water: rock
EBS-10*	182	–	21.11	316 SS	14.94	0.67	0.67	WB only	300	6 weeks	8:1
EBS-14	128	14.86	–	–	–	0.48	0.48	OC only	300	6 weeks	8:1
EBS-15	159	3.68	14.72	316 SS	12.63	0.59	0.59	–	300	6 weeks	8:1
EBS-17	155	3.61	14.44	Copper	12.21	0.58	0.58	–	300	6 weeks	8:1
EBS-19	120	3.70	14.82	304 SS	6.55	0.60	0.59	–	300	6 weeks	6:1
EBS-20	261	5.80	29.08	316 SS	6.60	0.95	0.95	–	300	6 months	7:1
EBS-21	126	2.63	10.47	316 SS	9.14	0.33	0.33	+ 1 M NaCl	200	8 weeks	9:1
EBS-22	132	7.29	7.30	316 SS	9.98	0.51	0.50	50:50 OC:WB	200	8 weeks	8:1

*EBS-10 is from Cheshire et al. (2014) and reported here for comparison

silica-saturated conditions (Cheshire et al. 2013, 2014) or clay-mineral reactions (Mosser-Ruck et al. 2010). Dissolution of clinoptilolite, which makes up roughly 13% of the Wyoming bentonite used in this study, and precipitation of analcime may result in a slight volume loss within the bentonite buffer (Cheshire et al. 2014).

Opalinus Clay

Opalinus Clay used in the present study was sourced from the Mont Terri Underground Rock Laboratory in Canton Jura, northern Switzerland. The rock used was from the shaley facies of Opalinus Clay at Mont Terri (drill core BFE-A10) and was exposed to air (i.e. oxidizing conditions) before the experiment. Opalinus Clay is considered to be a favorable medium for a repository based on its high clay content, low permeability, high sorption potential for radionuclides, and crack-sealing properties (NAGRA 2002; Bossart and Thury 2008; Bossart and Milnes 2017). Several experimental studies have examined the mineralogical and chemical evolution of Opalinus Clay at temperatures below 200°C. The interaction of high-pH fluids and Opalinus Clay had been evaluated at ambient (e.g. Adler et al. 1999; Taubald et al. 2000) and elevated (e.g. 90–200°C; Honty et al. 2012; Chermak 1992) temperatures. The presence of cement and/or high-pH solutions at ambient temperatures (25°C) results in the dissolution of the precursor chlorite in the Opalinus Clay (Taubald et al. 2000) and the formation of Ca-zeolites and calcium aluminum silicate hydrate minerals (Alder et al. 1999). At higher temperature (150–200°C) and similar pH, the formation of analcime, vermiculite, and Na-rectorite was observed within powdered Opalinus Clay (Chermak 1992). In situ EBS experiments at the Mont Terri underground research laboratory in Opalinus Clay are in progress (HE-E, up to 140°C; Wieczorek et al. 2017; FE, up to 150°C; Müller et al. 2018).

METHODS

Experimental

No previous experiments have been performed on the interaction of Opalinus Clay and Wyoming bentonite at elevated temperatures and pressures. Three systems were tested under water-saturated conditions: (1) Opalinus Clay only, (2) 80 wt.% bentonite with 20 wt.% Opalinus Clay, and (3) 50 wt.% all on the same line Opalinus Clay and 50 wt.% Wyoming bentonite (Table 1). The Opalinus Clay-only experiments provide a baseline for mineralogical reactions that occur at 300°C. The 20% and 50% Opalinus Clay experiments aimed to represent the interface zone between repository host rock and bentonite in order to characterize any host-rock–backfill interactions (Fig. 2). Some experiments included metal coupons to mimic the presence of a spent fuel waste canister. These experiments build on previous work by Cheshire et al. (2014) that included Wyoming bentonite-only hydrothermal experiments. Experiments were conducted at either 200 or 300°C to characterize a range of systems based on various maximum temperatures in generic repository designs. Experiment duration was varied to observe kinetic effects and/or to evaluate the attainment of steady state under the experimental conditions.

The Opalinus Clay and Wyoming bentonite were pulverized to <5 mm granules and sieved to <2 mm and >2 mm fractions. A synthetic groundwater solution was prepared to mimic the groundwater composition in equilibrium with Opalinus Clay (Pearson 2002; NAGRA 2002) using reagent-grade salts dissolved in double deionized water. This synthetic groundwater had a pH of ~7.5 and the initial chemistry is reported in Table 2. Additional 1 M (~22.9 g/L) NaCl solution (see below) was added to the Opalinus Clay solution in experiment EBS-21 to observe the influence of a saline brine.

Solutions were added at between 6:1 and 9:1 water:rock mass ratios. The redox conditions for each experiment were buffered using a 1:1 mixture (by mass) of Fe₃O₄ and Fe° filings that comprised ~0.5–0.9% of the total mass of the solid and liquid reactants. Coupons of 304 >stainless steel (NIST SRM 101g), 316 stainless steel (NIST SRM 160b), low-carbon steel (provided by Sandia National Laboratory), or Cu-foil (experiment EBS-17) were added to all experiments, except EBS-14. The mass of the metal pieces comprised ~4–7 wt.% of all reactants and were added in order to observe any mineral alteration and corrosion at the bentonite–coupon surface interface. Reactants (Table 1) were loaded into a flexible gold reaction cell and fixed
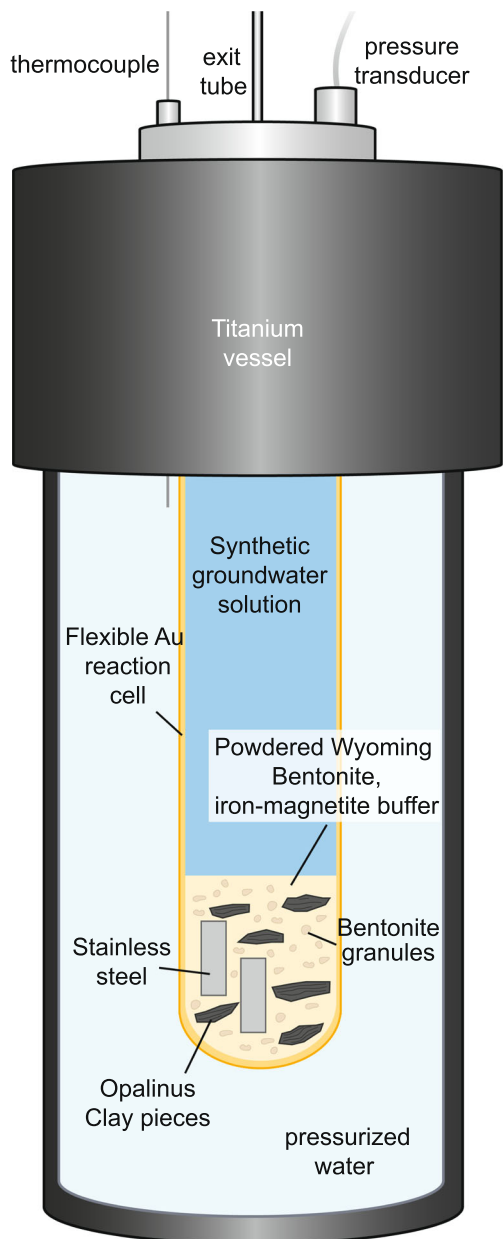
Fig. 2. Schematic of the experimental set up (not to scale).

Table 2. Brine compositions including the type solution for Opalinus Clay porewater from the Mont Terri site (Pearson 2002) and the composition of the synthetic solution created and used in the hydrothermal experiments.

	Type solution	Actual solution
Species	(mg/L)	(mg/L)
Ca^{2+}	421	426
Cl^-	5672	6470
CO_3^{2-}	162	n.m.
K^+	221	225
Mg^{2+}	182	194
Na^+	3885	3846
Si	5	1
SO_4^{2-}	2305	998
Sr^{2+}	27	0
TDS	11502	12153
pH	7.24	7.50

locally on the coupon surfaces, but did not extend more than ~50 μm perpendicular to the coupon surface. Corrosion and steel alteration results will be discussed in a separate article.

Characterization

Aqueous chemistry. Reaction liquids were sampled (4–5 g per sampling) weekly during the 6–8 week experiments and bi-monthly during the 6 month experiments. Fluid samples from the experiments were extracted in airtight syringes and often included gas phases. The gas phases were likely CO_2-dominated based on the lack of sulfur smell and the experimental components. In contact with ambient laboratory conditions, the reaction fluids quickly reached 25°C; salt precipitation was not observed during fluid cooling. An aliquot of the reaction fluids was used to measure immediately the pH at 25°C using a Thermo Orion 4 Star pH probe (Thermo, Waltham, Massachusetts, USA). The reaction liquids were divided into aliquots analyzed for unfiltered anion, unfiltered cation, and filtered (0.45 mm syringe filter) cation determination. All aliquots were stored in polytetrafluoroethylene vials and stored at 1°C before analysis.

Major cations and trace metals were analyzed via inductively coupled plasma-optical emission spectrometry (ICP-OES) (Optima 2100 DV, Perkin Elmer, Waltham, Massachusetts, USA) and inductively coupled plasma-mass spectrometry (ICP-MS) (Elan 6100, Perkin Elmer, Waltham, Massachusetts, USA) utilizing EPA methods 200.7 and 200.8 at Los Alamos National Laboratory. Ultra-high purity nitric acid was used in sample and calibration preparation prior to sample analysis. Internal standards (Sc for ICP-OES and Bi, In, and Y for ICP-MS) were added to samples and standards to correct for matrix effects. Standard Reference Material (SRM) 1643e Trace Elements in Water was used to check the accuracy of the multi-element calibrations. Inorganic anion samples were analyzed by ion chromatography (IC) following EPA method 300

into a 500 mL gasket-sealed reactor (Seyfried 1987) (Fig. 2). Experiments were pressurized to ~150 bar (mimicking hydrostatic pressures for a shallow repository) and were heated to either 200°C or 300°C for various lengths of time. Four 300°C experiments (EBS-14, EBS-15, EBS-17, and EBS-19) were run for 6 weeks and two 200°C experiments (EBS-21 and EBS-22) were run for eight weeks. One 300°C experiment (EBS-20) was run for 6 months.

Solid reaction products were extracted post experiment and dried at room temperature under oxidizing conditions. Metal coupons were extracted from the clay and rock components. Corrosion and metal alteration phases were observed

Table 3. Quantitative X-ray diffraction (XRD) results from the starting materials and the bulk reaction products (only stainless steel coupons were removed before sample powdering).

SAMPLE ID	WB	OC	80:20*	50:50*	EBS-14 OC only	EBS-15	EBS-17	EBS-19	EBS-20	EBS-21	EBS-22 50:50
			Starting Materials					80 WB:20 OC			
			Unheated					300°C			200°C
NON-CLAY FRACTION											
Quartz	1.5	13.8	3.9	7.6	7.2	3.9	3.0	3.9	4.0	3.3	6.1
K-Feldspar	0.7	5.9	1.8	3.3	0.6	0.9	0.9	1.0	1.1	0.9	1.2
Plagioclase	6.2	3.0	5.5	4.6	2.0	8.4	10.2	11.8	9.8	5.3	5.5
Apatite	0.0	0.0	0.0	0.0	0.8	0.0	0.8	0.7	0.5	0.5	0.8
Calcite	0.0	16.4	3.3	8.2	7.9	0.0	0.0	0.0	0.0	0.9	3.9
Dolomite	0.0	0.7	0.1	0.4	0.7	0.0	0.0	0.0	0.0	0.0	0.0
Gypsum	0.1	0.0	0.1	0.0	0.2	0.0	0.0	0.2	0.0	0.0	0.3
Halite	0.0	0.0	0.0	0.0	0.0	0.0	0.6	0.9	0.4	4.2	1.2
Anatase	0.0	0.0	0.0	0.0	0.5	0.0	0.0	0.1	0.1	0.1	0.4
Pyrite	0.2	1.1	0.4	0.7	0.2	0.3	0.4	0.3	0.3	0.1	0.2
Clinoptilolite	13.0	0.0	10.4	6.5	0.0	10.6	7.6	12.0	4.1	6.4	3.1
Analcime	0.0	0.0	0.0	0.0	2.9	0.9	2.6	0.3	0.8	0.0	0.0
Cristobalite	1.5	0.0	1.2	0.8	0.0	0.0	0.0	0.0	0.0	0.0	0.0
TOTAL	23.2	40.9	26.7	32.0	22.9	24.9	25.9	31.3	21.1	21.8	22.9
CLAY FRACTION											
Smectite + Illite + I-S	71.0	24.1	61.7	47.6	57.2	69.4	70.0	64.3	75.2	76.3	63.4
Mica	3.8	7.4	4.5	5.6	11.0	4.8	3.4	3.1	2.6	1.3	4.1
Chlorite	2.0	9.1	3.4	5.6	8.0	0.9	0.6	1.2	1.1	0.6	3.2
Kaolinite	0.0	16.9	3.4	8.5	0.9	0.0	0.0	0.0	0.0	0.0	6.3
TOTAL	76.8	57.5	73.0	67.2	77.1	75.1	74.1	68.7	78.9	78.2	77.1

*Representative compositions for the starting mixtures of Wyoming bentonite (WB) and Opalinus Clay (OC) are calculated from data at either an 80:20 or a 50:50 ratio.

on a Dionex DX-600 system (Thermo, Waltham, Massachusetts, USA). Aqueous chemical results are presented in Appendix 1. Typical 2σ uncertainties for the aqueous chemistry results are less than < ~5%. Geochemical evaluation of aqueous species activities and mineral saturation states were performed using *The Geochemist's Workbench* v.12 and *EQ3/6* (Wolery and Jarek 2003) software using the V8.R6+ and a modified version of the YMP thermodynamic database (Wolery and Jove Colon 2007). The geochemical evaluation was conducted using filtered cation and anion concentration data. Equilibrium aqueous speciation calculations were conducted by initially computing aqueous speciation of quench experimental fluids at 25°C followed by recalculation at the experimental temperatures (200–300°C). Speciation calculations assumed equilibrium with pCO_2 of $10^{-3.5}$ bars and charge balancing on Cl⁻. Calculations for solution pH and silica activity can be found in Appendix 3.

Scanning electron microscopy. Reaction products from each experiment were imaged using a FEI[TM] Inspect F scanning electron microscope (SEM) (FEI, Hillsboro, Oregon, USA) at Los Alamos National Laboratory. All samples were either Au- or C-coated prior to SEM analysis. Imaging with the SEM was performed using a 5.0–10.0 kV accelerating voltage and 1.5–3.0 nm spot size. Qualitative energy dispersive X-ray

spectroscopy (EDX) for mineral identification was performed at 30 kV and a 3.0–5.0 nm spot size using an EDAX Octane Elite silicon drift detector (AMETEK, Berwyn, Pennsylvania, USA).

X-ray diffraction (XRD). The mineralogy of the starting materials and bulk reaction products was determined by quantitative X-ray diffraction (QXRD). Only the metal coupons (if present) were removed before the reaction product samples were analyzed — the reacted Wyoming bentonite and Opalinus Clay fractions were analyzed together for the powder XRD analysis for EBS-15 through EBS-22. Samples were ground with 20 wt.% corundum (Al_2O_3) for analysis of the bulk rock (Chung 1974). Powder mounts were prepared for QXRD measurements, which were conducted using a Siemens D500 diffractometer (Siemens, Munich, Germany) with CuKα radiation. Data were collected from 2 to 70°2θ with a 0.02°2θ step size and count times of 8 to 12 s per step. QXRD data were determined using *FULLPAT* (Chipera and Bish 2002) (Table 3). Typical 2σ uncertainties of the *FULLPAT* method were ~3.4% (Chipera and Bish 2002).

The clay mineralogies of the reacted Wyoming bentonite and Opalinus Clay fractions were also characterized. Discrete Opalinus Clay shale fragments (~1–5 mm) were separated manually from the fine-grained clay matrix composed of

mostly Wyoming bentonite. The clay matrix was dominantly Wyoming bentonite, but may have contained trace amounts of Opalinus Clay powder. The Opalinus Clay fragments were sonicated in DI water to remove clay groundmass material before crushing. The separate sample fractions of Wyoming bentonite and Opalinus Clay fragments were crushed gently by hand in an agate mortar and pestle. The <2 μm particles from each sample were separated via sedimentation in deionized (DI) H$_2$O. A portion of the <2 μm suspension was dropped on a zero-background quartz plate, dried on a hot plate at 60°C to create an oriented clay mount, and X-rayed from 2 to 40°2θ angle with a step size of 0.02 at 8 to 12 s per step. The oriented clay mount was then saturated with ethylene glycol in a 60°C oven for 24 h and the XRD analysis was repeated.

Electron microprobe analyses. Electron microprobe (EMP) analyses were performed at the University of Oklahoma using a Cameca SX50 electron microprobe (CAMECA, Gennevilliers, France) equipped with five wavelength-dispersive spectrometers and a PGT PRISM 2000 energy-dispersive X-ray detector. Quantitative analysis was performed by wavelength-dispersive spectrometry using 20 kV accelerating voltage, 20 nA beam current, and 2 μm spot size. Matrix corrections employed the PAP algorithm (Pouchou and Pichoir 1984), with oxygen content calculated by stoichiometry. Counting times were 30 s on peak for all elements, yielding minimum levels of detection (calculated at 3σ above mean background) in the range of 0.01 to 0.03 wt.% of the oxides for all components except F (0.16 wt.%). All standards for elements in the silicates were analyzed using 30 s count times on the peak, using K-alpha emissions. Mineral standard information and oxide detection limits can be found in Appendix 2. Typical uncertainties for the EMP analyses were <1% based on long-term standard reproducibility.

RESULTS

Aqueous Chemistry

The experimental parameters that likely had the greatest effect on the evolution of the solution chemistry were salinity, temperature, and water:rock ratio. The 200 and 300°C experiments started with a near neutral pH (25°C) of 7.5 (Table 2). The solution pH for all experiments generally dropped within the first three weeks (Fig. 3). The 200°C experiments ended with pH values at 25°C between 5.5 and 6. The 300°C experiments with a water:rock ratio between 7:1 and 8:1 (EBS-14, EBS-15, EBS-17, EBS-20) reached pH (25°C) values between 5 and 5.5 (Fig. 3). Experiment EBS-19 had a water:rock ratio of ~6:1; solution chemistry evolved at slightly higher pH values (pH ~6) in comparison to the other 300°C runs (Fig. 3). The recalculated pH values at 300°C were between 4.3 and 5.7 and at 200°C values were ~5.5. Plots for cation and anion concentrations can be found in the Supplementary Materials. As expected, the addition of 1 M NaCl to the starting solution of EBS-21 resulted in much higher [Na$^+$] and [Cl$^-$] in comparison to the other experiments. Further, [Ca^{2+}], [SO$_4^{2-}$], [Fe^{2+}], and [Al^{3+}] are elevated in comparison to all other results. Aqueous silica remained below detection in EBS-21.

Sodium and potassium concentrations in the 300°C experiments and EBS-22 covered a wide range of values. Variation between experiments is not readily explainable by differing experiment materials or water:rock ratios. For example, the sodium concentrations remained near initial groundwater concentrations of 4000 mg/L in EBS-14, EBS-17, EBS-20, and EBS-22. Sodium concentrations decreased to ~2500 mg/L in EBS-15, but increased to ~7500 mg/L in EBS-19. Increased cation concentrations in EBS-19 may be due to a lower water:rock ratio (6:1); however, EBS-15 and EBS-17 had the same starting components and water:rock ratio.

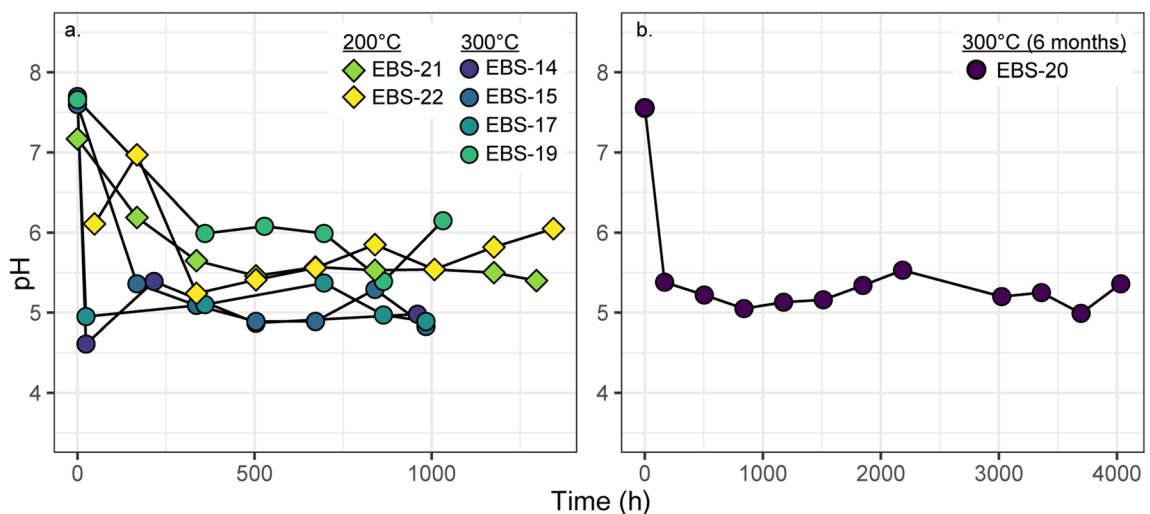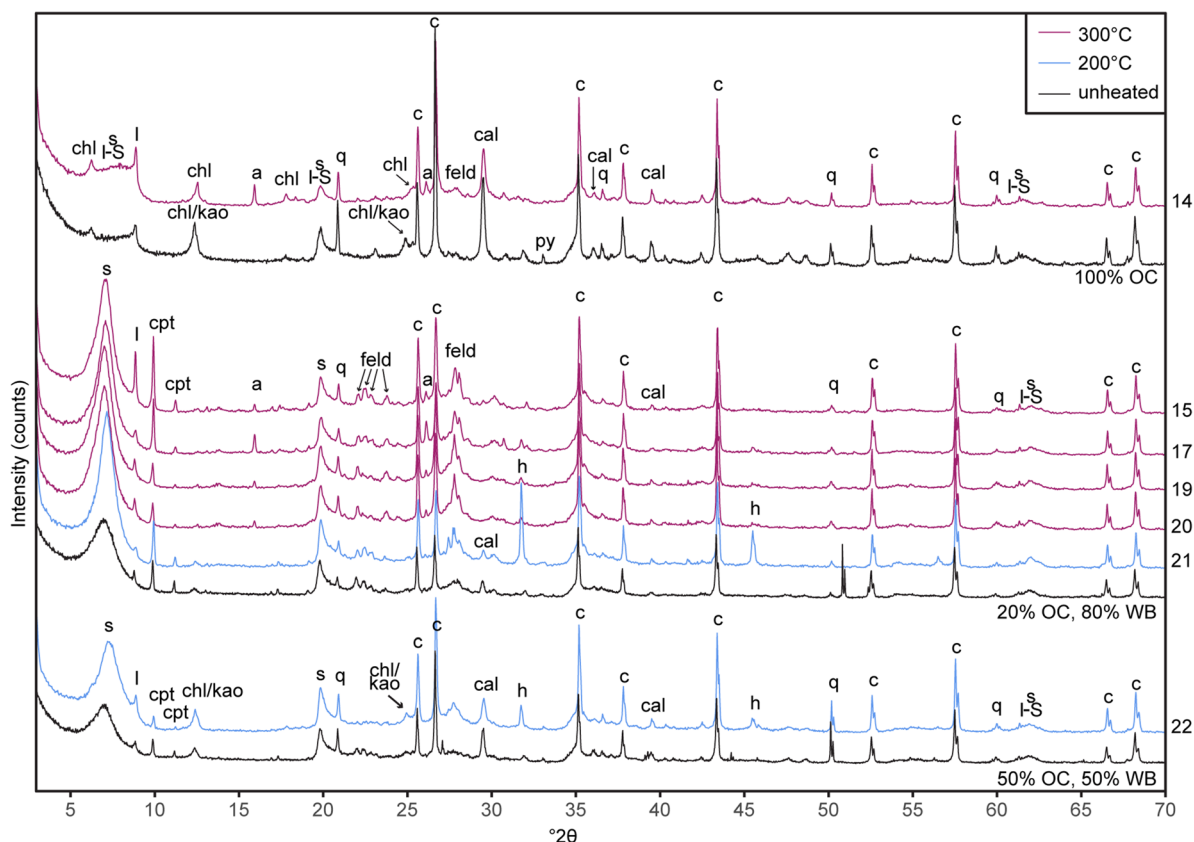**Fig. 3.** pH (at 25°C) evolution of **a** 6–8-week and **b** 6-month experiments.

Fig. 4. Powder XRD patterns of the bulk reaction products and starting Wyoming bentonite (WB) used for calculating mineral abundances. Peaks corresponding to smectite (S), clinoptilolite (cpt), analcime (a), feldspar (feld), illite-smectite (I-S), chlorite (chl), illite (I), kaolinite (kao), quartz (Q), calcite (cal), halite (h), and corundum (c) (internal standard) are labeled.

Calcium concentrations decreased with respect to starting solution values (426 mg/L) in experiments with an Opalinus Clay–Wyoming bentonite mixture to values between 100 and 200 mg/L. In comparison, in the Opalinus Clay-only experiment (EBS-14), Ca^{2+} concentrations increased to ~550 mg/L all on the same line mg/L by the end of the experiment.

Dissolved silica concentrations increased rapidly to >100 mg/L from starting solution values of 2 mg/L by the first sample extraction in all experiments except EBS-21. Aqueous SiO_2 concentrations in all the 300°C experiments remained generally constant between 100 and 200 mg/L throughout the duration of the experiment. In EBS-22, aqueous silica reached between 300 and 400 mg/L after 200 h of experiment time.

Iron and aluminum concentrations in EBS-15 through EBS-20 generally increased. Aluminum [Al^{3+}] concentrations were below detection limits in EBS-14 and EBS-22. The 300°C Opalinus Clay and Wyoming bentonite experiments at 300°C (EBS-15 through 20) showed [Al^{3+}] below ~0.5 mg/L. Iron concentrations generally remained below 0.5 mg/L during the experiments, with the exception of EBS-21 (saline-brine experiment). In contrast, Mg decreased during all experiments from starting concentrations of ~200 mg/L to <5 mg/L.

Quantitative X-ray Diffraction (QXRD)

The QXRD results show that unreacted Opalinus Clay was composed dominantly of illite, illite-smectite, kaolinite, calcite, quartz, chlorite, and biotite with lesser feldspar (plagioclase and potassium feldspar) and minor dolomite, pyrite, and siderite (Fig. 4, Table 3). The starting Wyoming bentonite was dominantly smectite (Na montmorillonite), with lesser clinoptilolite and plagioclase, and minor quartz, pyrite, and biotite. Powder XRD patterns for unheated Opalinus Clay and the Opalinus Clay–Wyoming bentonite mixtures are plotted in Fig. 4.

The mineral groups present in significant amounts (>5 wt.%) in all of the reaction products included clays, feldspars, zeolites, and/or phyllosilicates, with lesser SiO_2 polymorphs and/or carbonates. Other minerals identified to make up <5% in all samples included gypsum, halite, K-feldspar, magnetite, and/or pyrite. Native iron, added as a part of the iron-magnetite oxygen fugacity buffer, was observed in sample thin sections and SEM images, but was not detected in the QXRD results, likely due to its low abundance in the bulk mineralogy.

Clay minerals were the most abundant phase in all of the reaction products and were a combination of illite, smectite, mixed illite-smectite, chlorite, mica, and/or kaolinite. Illite, interstratified illite-smectite, and smectite were grouped
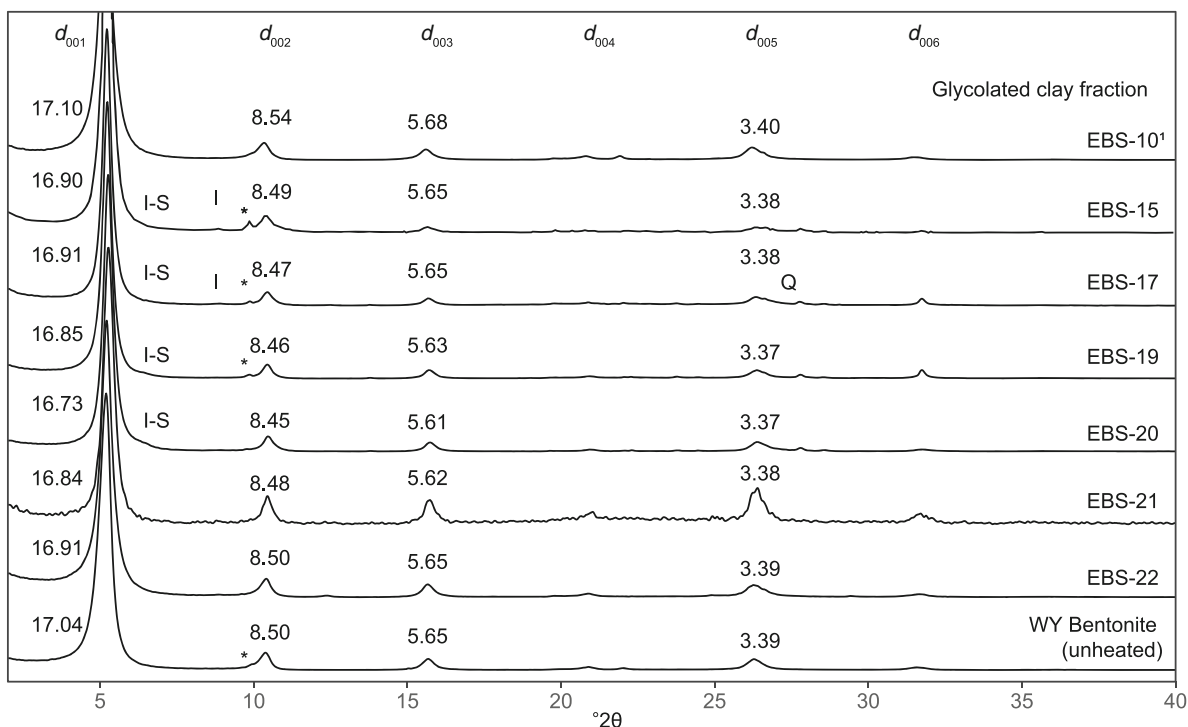
Fig. 5. XRD results from the oriented, ethylene glycol-saturated clay fraction of the bentonite groundmass for all experiments and unreacted Wyoming bentonite. The positions of chlorite-smectie (C-S), glycolated smectite (numbered), illite (I), illite-smectite (I-S), and quartz (Q) peaks are indicated. [1]Data from EBS-10 (Cheshire et al. 2014) are plotted for comparison. *Clinoptilolite peak around 8.9 Å.

together due to the difficulty of distinguishing between these phases in the powder XRD patterns (Table 3). Combined illite, illite-smectite, and smectite ranged between 57 and 76 wt.% in the reaction products. Mica was observed to be 1–11 wt.% and chlorite was 1–8 wt.%, whereas kaolinite was observed in EBS-14 (1 wt.%) and EBS-22 (6 wt.%).

The QXRD results indicated the presence of plagioclase and/ or K-feldspar in all experiment products. For all of the experiments, the reaction products had ~1–2 wt.% K-feldspar. Plagioclase feldspar made up between ~2 and 12 wt.%. Quartz made up between 3 and 7 wt.% of the reaction products.

Zeolite minerals identified in the reaction products were dominantly clinoptilolite, with lesser analcime–wairakite. Clinoptilolite was not present in EBS-14 (pure Opalinus Clay), but comprised ~8–12 wt.% of EBS-15, EBS-17, and EBS-19 samples. Samples from EBS-20 through EBS-22 had ~3–6 wt.% clinoptilolite. Analcime–wairakite solid solution was detected in 300°C experiments (EBS-14 through EBS-20; ~0.3-2.9 wt.%), but was not observed in the 200°C reaction products (EBS-21 and EBS-22).

The powder XRD patterns highlight changes in the bulk, reaction-product mineralogy in comparison to the patterns from the starting materials (Fig. 4). The run-product mineralogy of EBS-14 (Opalinus Clay only, 300°C) compared to unheated Opalinus Clay showed the reduction in kaolinite and calcite and the appearance of analcime peaks. The illite

peak in EBS-14 was also sharper and narrower in comparison to the starting Opalinus Clay, potentially indicating precursor illite recrystallization and/or new illite crystallization. The 300°C experimental products in the mixed Opalinus Clay– Wyoming bentonite systems also showed the appearance of analcime peaks, whereas the 200°C systems and starting materials (20:80 and 50:50) lacked this zeolite. Calcite peaks were reduced in intensity in the 300°C run products in the mixed systems, but were comparatively unchanged in the 200°C products (Fig. 4). The d_{060} region of the XRD results did not show evidence of newly formed trioctahedral minerals; peaks remained near 1.50 Å in the run products from EBS-15 through EBS-22 (Fig. 4).

Clay Mineral X-ray Diffraction (XRD)

Oriented air-dried and ethylene glycol-saturated mounts of the < 2 μm clay fraction were analyzed in order to examine clay-mineral transformations. The XRD patterns from the reacted and unreacted materials reflected mainly clay-mineral changes under experimental conditions. The fine-grained clay groundmass of the experimental products, which included mainly Wyoming bentonite with a small amount of Opalinus Clay powder, and discrete fragments of Opalinus Clay were separated and analyzed (Figs 5 and 6).
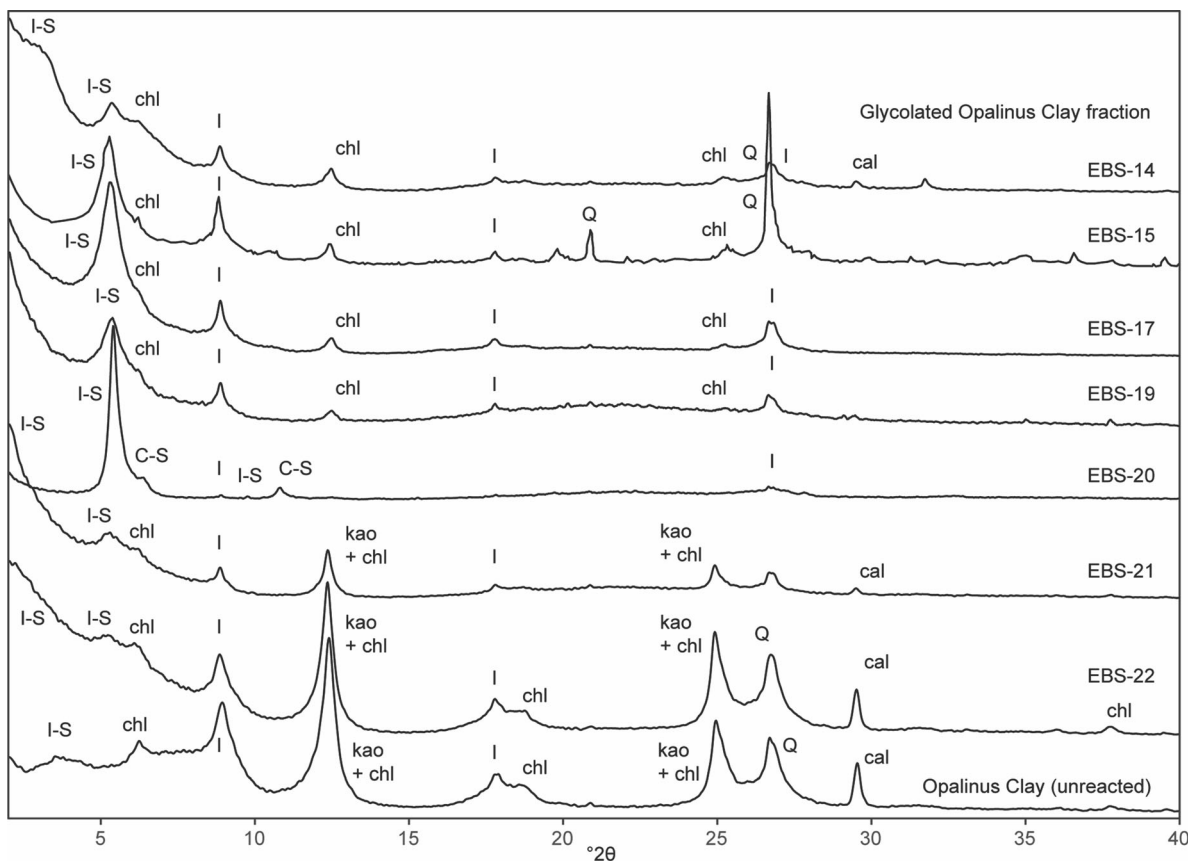
Fig. 6. XRD results from the oriented, ethylene glycol-saturated clay fraction of Opalinus Clay fragments extracted from each experiment and unreacted Opalinus Clay. Peaks corresponding to illite-smectite (I-S), chlorite (chl), illite (I), kaolinite (kao), quartz (Q), and calcite (cal) are labeled.

Clay groundmass. Peak patterns from the ethylene-glycolated clay fraction from unreacted Wyoming bentonite and the clay fraction separated from the groundmass (mainly Wyoming bentonite, with trace amounts of Opalinus Clay) products of experiments EBS-15 through EBS-22 were characteristic of ethylene glycol-saturated montmorillonite (Fig. 5). The XRD results from unreacted Wyoming bentonite were compared to the reaction products from the present study and an example (EBS-10) from Cheshire et al. (2014) (Fig. 5). Experiment EBS-10 from Cheshire et al. (2014) was conducted under the same experimental conditions, but with Wyoming bentonite only. The XRD results from the bentonite and Opalinus Clay experiments showed minimal smectite alteration. Hydrothermal treatment resulted in the reduction of the glycolated-smectite d_{001} values by between 0.1 and 0.3 Å. However, expandability estimates based on the position of the d_{002}/d_{003} ethylene glycol-saturated peak positions indicated no reduction of swelling capacity of the montmorillonite in the 6week, 300°C experiments (EBS-15, EBS-17, and EBS-19) (Table 4). The 6-month experiment (EBS-20) showed a slight reduction in expandability in comparison to unreacted bentonite (~2% decrease). The experiment conducted at 200°C with a saline brine (EBS-21) showed a similar reduction in

expandability to EBS-20, whereas the other 200°C experiment (EBS-22) showed no change. The difference between the d_{002} and d_{003} ethylene glycolated peak positions can also be used to estimate the percentage of illite in illite-smectite mixed layers. Using the calibration based on the difference in the d_{003} and d_{002} ethylene glycol-saturated illite-smectite peaks presented in Leupin et al. (2014), only the EBS-20 clay groundmass contained detectable illite-smectite mixed layers (~1%) (Table 4). Either the formation of interlayered illite or, more likely, the physical mixture of illite derived from the Opalinus Clay is responsible for the slight decrease in smectite expandability in EBS-20.

Opalinus Clay fragments. Unreacted Opalinus Clay contained diverse clay and phyllosilicate minerals including illite, illite-smectite interstratified minerals, chlorite, and kaolinite (Table 3, Fig. 6). The XRD patterns of heated Opalinus Clay fragments separated from the reaction products indicated that several clay mineral transformations had occurred. In all results, mineral quantification was hindered by the presence of various mixed-layer phases.

The Opalinus Clay fragments in EBS-22 retained the same chlorite, kaolinite, and calcite peaks as the precursor materials. The results from EBS-21 showed similar XRD patterns, but with
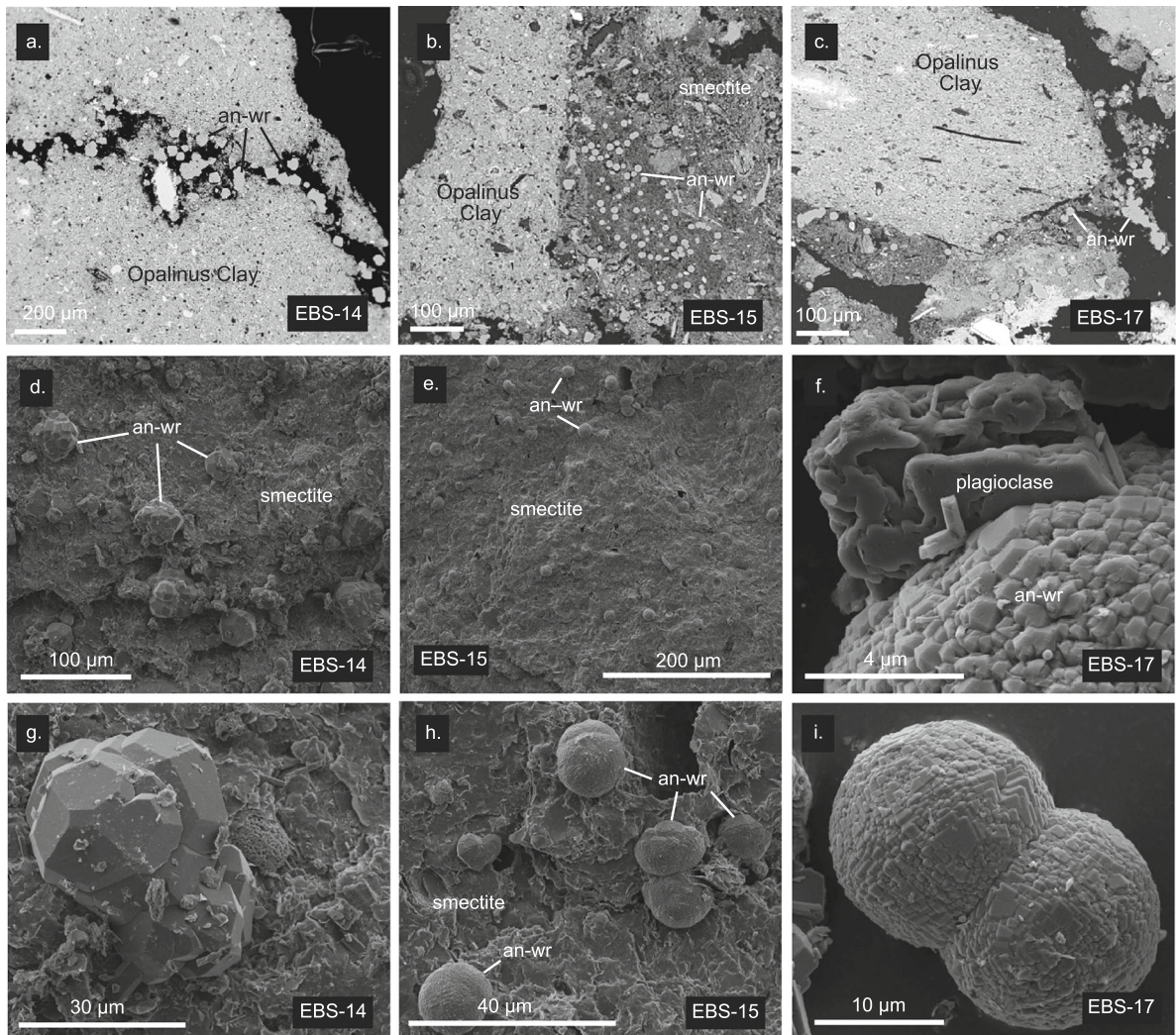
Fig. 7. Representative SEM images from 300°C experiments with Opalinus Clay ± Wyoming bentonite. **a–c**: Backscatter-electron SEM thin-section images of 300°C experiments with (**a**) Opalinus Clay only (EBS-14) and (**b,c**) Opalinus Clay + Wyoming bentonite in EBS-15 and EBS-17. Analcime–wairakite (an–wr) crystals form either on cracks/edges of Opalinus Clay fragments and/or dispersed within the bentonite clay matrix. **d–i**: Secondary electron images of reaction products. (**d**) Analcime–wairakite crystals on the surface of an Opalinus Clay fragment. (**e**) Analcime–wairakite dispersed in smectite. (**f**) Newly formed analcime-wairakite and corroded albite (plagioclase). (**g, h, i**) Analcime–wairakite crystals from the 300°C, 6-week experiments.

reduced intensity kaolinite and calcite peaks. In both, the main alteration signature was the shift of the low-angle reflections that indicated the presence of interstratified illite-smectite minerals (Fig. 6).

In the 300°C, 6-week experiments, the XRD patterns of Opalinus Clay fragments were characterized by mixed-layer illite-smectite, illite, and chlorite (Fig. 6). The 6-month experiment (EBS-20) showed a signature which was significantly different from the shorter 300°C experiments. Mixed-layer illite-smectite was present, likely 60% illite with 30–39% expandability based on the spacing of the d_{002} and d_{003} ethylene glycol-saturated peaks. The discrete illite peak around 10 Å was reduced to a minor peak. Peaks corresponding to

chlorite were no longer observed. Instead, peaks corresponding to mixed-layer chlorite-smectite were present (Fig. 6).

Scanning Electron Microscopy (SEM)

300°C experiments. Analcime–wairakite crystals in the 300°C reaction products were observed either rimming fragments of Opalinus Clay or within the fine-grained bentonite clay matrix (Fig. 7a–c). Secondary electron images of the analcime–wairakite revealed that these crystals were commonly embedded within a recrystallized smectite matrix (Fig. 7d, e, g, and h). Recrystallization of clay minerals was evident within the SEM images. In some experiments, the analcime–wairakite was associated

Table 4. Peak positions for ethylene glycol-saturated smectite for unheated Wyoming Bentonite and the clay fraction of the groundmass (Wyoming bentonite with trace Opalinus Clay) from the reaction products (EBS-15 through EBS-22). Expandability was calculated using three equations based on the separation between the d_{002} and d_{003} peak positions.

Ethylene gycolated smectite	001		002		003		004		005		002/003	1	2	3	%I*
Sample	d (Å)	2θ	d (Å)	2θ	d (Å)	2θ	d (Å)	2θ	d (Å)	2θ	Δ 2θ	%Exp	%Exp	%Exp	Δ 2θ
WY Bentonite	17.04	5.18	8.50	10.40	5.65	15.66	4.24	20.92	3.39	26.30	5.26	100	102	103	0
EBS-15	16.90	5.22	8.49	10.45	5.65	15.66	4.26	20.83	3.38	26.30	5.25	100	102	103	0
EBS-17	16.91	5.22	8.47	10.44	5.65	15.66	4.25	20.86	3.38	26.30	5.22	102	105	105	0
EBS-19	16.85	5.24	8.46	10.44	5.63	15.72	4.24	20.94	3.37	26.40	5.28	99	100	101	0
EBS-20	16.73	5.28	8.45	10.46	5.61	15.76	4.23	20.98	3.37	26.42	5.30	98	99	100	1
EBS-21	16.72	5.28	8.47	10.44	5.63	15.72	4.22	21.02	3.37	26.40	5.28	99	100	102	0
EBS-22	16.92	5.22	8.50	10.40	5.65	15.66	4.25	20.88	3.39	26.24	5.26	100	102	103	0

1: %Exp = 973.76 − 323.45Δ + 38.43Δ² − 1.62Δ³ (Eberl et al. 1993)

² 2: %Exp = 1517.8 − 548.49Δ + 68.35Δ − 2.90Δ³ (Eberl et al. 1993)

3: %Exp = 766.01 − 194.10Δ + 12.924Δ² (Moore and Reynolds 1997)

*Determined based on the NEWMOD calibration curve presented by Leupin et al. (2014)

with feldspar grains that show dissolution textures (Fig. 7f).

200°C experiments. Smectite in the 200°C experiments was fine-grained and had less ordered textures than the montmorillonite reacted at 300°C (Fig. 8a, b). Pockets of pyrite were more prevalent than in the 300°C samples (Fig. 8a, c). Large calcite grains (possibly shell fragments) were observed, and, in some cases, pyrite grains were contained within calcite (Fig. 8c). Analcime–wairakite crystals were not identified.

Electron Microprobe Analyses (EMPA)

Electron microprobe analyses primarily targeted zeolite minerals (clinoptilolite and analcime–wairakite) found in the reaction products. The results of the microprobe analyses are reported in Appendix 2.

In general, the zeolite minerals formed in the 300°C experiments had intermediate compositions between analcime ($NaAlSi_2O_6 \cdot H_2O$) and wairakite ($CaAl_2Si_4O_6 \cdot 2H_2O$) endmembers. The results are plotted in Fig. 9 and compared

with results from Wyoming bentonite-only experiments (Cheshire et al. 2013). Analcime–wairakite from experiments with Opalinus Clay and Wyoming bentonite (EBS-15 through EBS-20) had a relatively limited range of Si/Al ratios between ~2.5 and 3.0 and Na/(Na + Ca) values of 0.52–0.64 (Fig. 9). In comparison, the analcime–wairakite formed in the experiment with only Opalinus Clay (EBS-14) had the lowest Si/Al ratio (~2.2) and Na content (Na/(Na + Ca) = 0.22). Clinoptilolite observed in EBS-21 had similar compositions to clinoptilolite from earlier EBS experiments and unreacted clinoptilolite.

DISCUSSION

The hydrothermal interaction of Wyoming bentonite and Opalinus Clay wall rock with synthetic groundwater was examined in this set of experiments with varying temperature, water chemistry, and starting components. The diverse reaction products demonstrated the effects of these changing parameters.
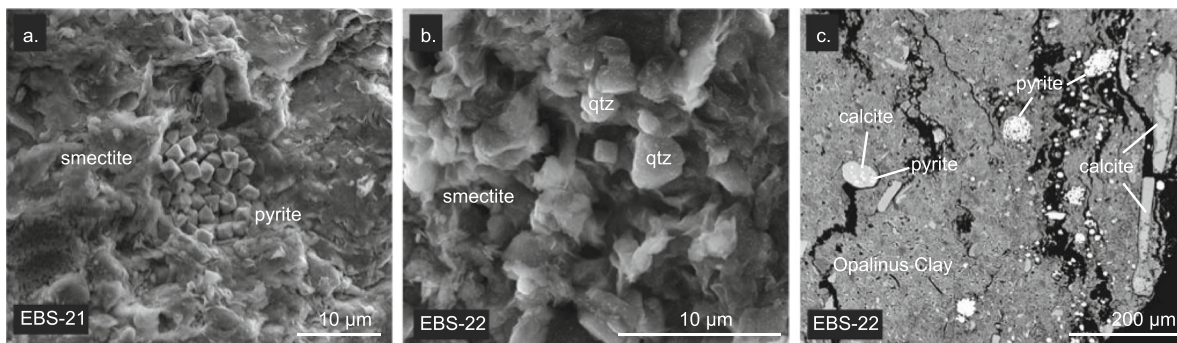
Fig. 8. Reaction products from the 200°C hydrothermal experiments. (**a**) Pockets of framboidal pyrite in an Opalinus Clay fragment (secondary electron image) in EBS-21. (**b**) Quartz crystals with smectite in the clay groundmass of EBS-22 (secondary electron image). (**c**) Calcite and pyrite in an Opalinus Clay fragment from EBS-22 (back-scatter electron).
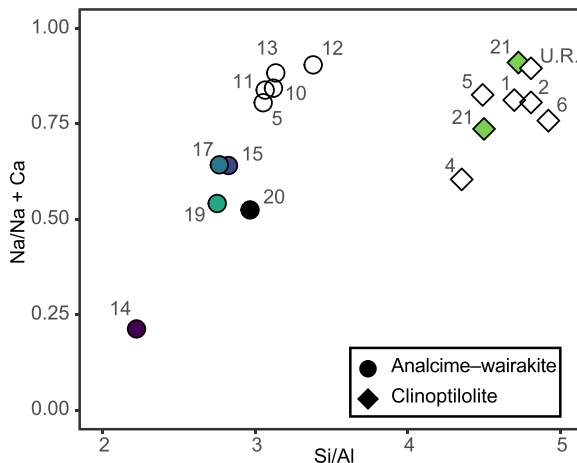
Fig. 9. Zeolite compositions from the present study (filled shapes, EBS-14 through EBS-21) and from Cheshire et al. (2013) (open shapes, EBS-1 through EBS-13). The numbers represent the EBS experiment identifier. The run conditions are as follows: 1–4, 6: 4- to 5-week bentonite-only experiments with a ramped thermal profile (25/100/200/300/25°C); 5, 10–13: 6-week bentonite-only at 300°C; 14: Opalinus Clay only for 6 weeks at 300°C; 15–20: Opalinus Clay + bentonite 6- to 8-week experiments at 300°C; and 21: Opalinus Clay + bentonite 200°C experiments. Bentonite-only experiments generally have higher Na/Na+Ca and Si/Al values. Experiments with Opalinus Clay shift to lower Si/Al and Na values.

Aqueous Chemistry

Aqueous cation and anion compositions largely reached steady-state conditions (i.e. constant measured values) after ~400 h of experiment time. Evolution of solution chemistry during the experiments probably reflected mineral–brine reactions. For example, [Ca^{2+}] was elevated in EBS-14 (Opalinus Clay only) in comparison to 300°C experiments wich contained Opalinus Clay and Wyoming bentonite mixtures. The increase in Ca^{2+} was likely related to calcite dissolution, which was observed in all 300°C experiments in the SEM and QXRD results. The higher concentrations in EBS-14 were likely due to the higher proportion of Opalinus Clay and, therefore, larger amount of calcite in the starting materials (~16 wt.%) in comparison to the mixed system (~3 wt.%). Increases in aluminum in solution were observed in the mixed systems and likely were related to reactions with aluminosilicate mineral formation (e.g. clay, feldspar, and zeolite) in the bentonite as aqueous aluminum concentrations were below the detection limit in the Opalinus Clay-only experiment. Similarly, iron increased throughout the experiments that contained Wyoming bentonite, but not in EBS-14, in which aqueous iron was below the detection limit. Observed iron concentrations are similar in all 300°C experiments with Wyoming bentonite, indicating that iron was likely sourced from mineral dissolution (e.g. pyrite) in the bentonite and/or the iron buffer materials, rather than the stainless steel or Opalinus Clay. The steel coupons included in the experiments likely did not contribute in a significant way to aqueous iron. Experiment EBS-17 included a copper foil

(no steel coupon) and observed iron concentrations were similar to those from experiments that included steel material (e.g. EBS-15, EBS-19, and EBS-20). Potential mechanisms of iron release include breakdown of chlorite and pyrite. Overall, the solution chemistries of experiments with similar components and *P-T* conditions show significant differences, further demonstrating the complexity of these experimental systems.

The pH of all experimental systems remained below 6.5, which is outside the carbonate buffer range. Calcite dissolution occurred based on the XRD and SEM observations and CO_2 gas was generated and extracted during fluid sampling. The recalculated pH values at temperature for all solutions were between 4.3 and 5.5, assuming initial ambient pCO_2 ($10^{-3.5}$ bar) conditions, indicating that the solution chemistry was likely buffered by a mineral system other than carbonate (e.g. Al-Si minerals; Gailhanou et al. 2017). Dissolved carbonate in the system could also influence the pH of the hydrothermal solutions. For example, calcite solubility is expected to be high at these *P-T* and pH conditions; therefore, dissolution of preexisting calcite in the Opalinus Clay rock may have contributed to the low observed pH. Also, other experimental studies have also shown decreases of pH in hydrothermal systems containing montmorillonite or clay rock (e.g. Johnston and Miller 1984; Heimann 1993; Gailhanou et al. 2017). Moreover, zeolite-forming reactions in low-temperature experiments with Opalinus Clay were also observed at lower solution pH (Adler et al. 1999). The EQ3/6 geochemical calculations showed that the reaction solutions were either saturated or supersaturated with respect to clays and Na-/Ca-clinoptilolite; therefore, the
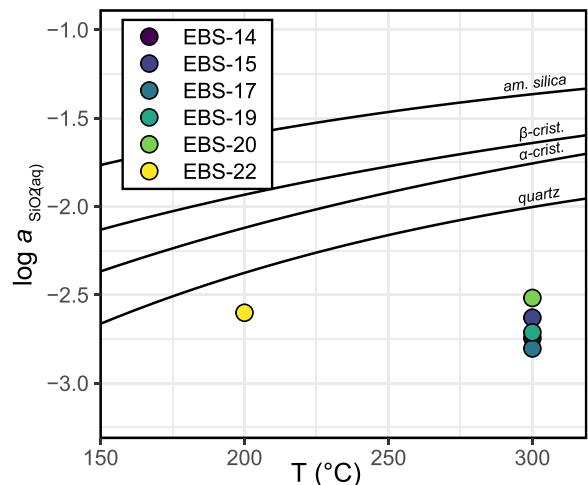
Fig. 10. Steady-state silica activity versus temperature for the 200°C (EBS-22) and 300°C (EBS-14, -15, -17, -19, and -20). Opalinus Clay + Wyoming bentonite 300°C and 200°C experiments remained undersaturated with respect to quartz. Data from EBS-21 are not shown as silica remained below the detection limit until the experiment quench. Silica saturation data are from (Rimstidt and Barnes 1980). Am., amorphous; crist., cristobalite.

reactions between brine and clay and/or zeolite likely buffered the solution pH in the experimental system.

Silica saturation has been identified as a major factor in the alteration of EBS materials (Smyth 1982; Bish and Aronson 1993; Neuhoff and Ruhl 2006; Cheshire et al. 2014). The presence of Opalinus Clay wall rock and synthetic groundwater had significant effects on the aqueous chemistry of the system, in particular, on the silica saturation state throughout each experiment. Cheshire et al. (2014) observed saturation with respect to cristobalite throughout the duration of 300°C Wyoming bentonite-only experiments (EBS-10, Fig. 10). In comparison, the aqueous chemical measurements from the 300°C Opalinus Clay ± Wyoming bentonite experiments of this study showed similar silica concentrations throughout each experiment, regardless of the proportions of starting material. That is, experiments having Opalinus Clay:Wyoming bentonite ratios of 100:0 and 20:80 showed similar $SiO_{2(aq)}$ concentration values (Fig. S1). The silica measurements correlated to calculated activities at the experimental temperature of 300°C to be below quartz saturation (Fig. 10).

In the 200°C experiments, silica remained below the detection limit in EBS-21 until after ~1100 h, and then increased to ~100 mg/L after experiment cooling (undersaturated with respect to quartz). In comparison, the aqueous fluids from EBS-22 indicated under saturation with respect to steady-state conditions. Based on the silica concentrations and the pH of the experimental system, dissolved silica was dominantly in the form of $SiO_2(aq)$ and derived from dissolution of precursor quartz and other silicate minerals from the reactant materials. Silica saturation can exert significant effects on the mineralogical evolution of materials, including clay mineral reactions and zeolite formation, which are discussed in the following sections.

Clay Mineral Alteration

The QXRD results and powder diffraction patterns from the bulk reaction products, in comparison to the XRD characteristics of the starting mixtures of Opalinus Clay and Wyoming bentonite, overall showed increased clay content (Table 3). XRD patterns of the oriented clay fraction from the reaction product groundmass provided insight into the structure of the clay phases present, differentiating between smectite, illite-smectite, and illite. The reaction products were characterized by peaks that align with ethylene glycol-saturated montmorillonite and showed minor shifts in comparison to peak positions of unreacted Wyoming bentonite (Fig. 5). Only EBS-20, the 6-month 300°C experiment showed a slight decrease in expandability (~2%) and detectable interlayered illite in interstratified illite-smectite (~1 wt.%) based on the ethylene glycol-saturated peak positions (Fig. 5, Table 4). Observed differences between the 6-week and 6-month experiments demonstrated the effect of reaction time on the mineralogical changes. The shifts in the peak patterns

in the results from the clay groundmass of EBS-20 cannot be attributed definitively to alteration of montmorillonite from Wyoming bentonite, as traces of Opalinus Clay powder and/or fragments, which contain precursor illite, may have remained. Therefore, given the very slight (~1%) estimated amount of interlayered illite in interstratified illite-smectite, the illitization of Wyoming bentonite montmorillonite over the 6-month period was likely negligible.

The clay mineral XRD results from the two 200°C experiments (EBS-21 and EBS-22) also reflect little change to the montmorillonite structure. With the addition of the highly saline brine in EBS-21, some reduction in montmorillonite expandability and kaolinite dissolution was observed. No discrete illite formation was observed in the analyzed 200°C clay fractions.

The observation of illite and illite-smectite in these experiments indicated that the presence of Opalinus Clay, which contains illite, may influence its nucleation in the EBS material. For example, discrete, newly formed illite in the clay groundmass of EBS-15 and EBS-17 likely nucleated on preexisting illite crystallites derived from the Opalinus Clay. The bulk composition of the system may have limited illitization of the Wyoming bentonite montmorillonite: cation exchange capacity measurements of bulk-rock Opalinus Clay samples reveal small values of exchangeable K^+ in comparison to values for Ca^{2+}, Na^+, and Mg^{2+} (Pearson et al. 2003). These results agreed with previous investigations that found the alkali chemistry of the system (i.e. low K^+) limits the formation of illite (e.g. Kaufhold and Dohrmann 2009; Cheshire et al. 2014). Low silica activities, however, likely favored illite stability and formation through the alteration of montmorillonite to illite, e.g. through the generalized reaction (Pusch et al. 1998; Pusch 2001; Cheshire et al. 2014):

$$\text{Na-montmorillonite} + K^+ + Al^{3+} \rightarrow \text{illite}$$
$$+ SiO_{2(aq)} + Na^+ + H_2O \qquad (2)$$
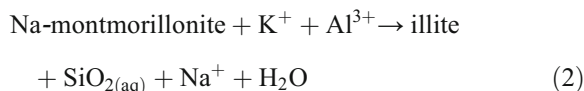
Montmorillonite dissolution textures were not prevalent from SEM observations and interstratified illite-smectite mineral formation in the clay groundmass was not detected. However, low levels of aqueous silica indicated that the reaction above was thermodynamically favored (Cheshire et al. 2014; Savage et al. 2019). Montmorillonite alteration was likely kinetically slow, as demonstrated by the small difference between the expandability estimates from the 6-week and 6-month experiments. Increased solute concentration was observed to accelerate clay-mineral reactions (Kasbohm et al. 2005), which was observed in EBS-21 having similar montmorillonite structural characteristics to the 6-month experiment.

The clay mineralogy of the Opalinus Clay fragments was altered significantly during the 300°C experiments; however, it remained comparatively unaltered in the 200°C experiments (Fig. 6). Kaolinite and calcite were reactive at 300°C, but stable during the 200°C experiments. Significant differences in the

clay fraction were observed between the Significant differences in the clay fraction 6-week and 6-month experiments at 300°C. Discrete chlorite and illite dominated the pattern of EBS-15, EBS-17, and EBS-19, whereas illite-smectite and chlorite-smectite mixed-layer minerals were the main phases in EBS-20 (Fig. 6). The increased presence of clay with some expansion capacity (i.e. presence of smectite) indicates that hydrothermal reactions in the host rock may increase favorable properties. However, host-rock temperatures will likely not reach 300°C in a deep geological disposal scenario as most repository design concepts limit drift-wall temperatures to <100°C (Greenberg et al. 2013).

The lack of montmorillonite alteration in Wyoming bentonite during interaction with Opalinus Clay rock and synthetic groundwater is a significant observation in the chemical environment of this experimental system. As mentioned above, silica under-saturation is thought to favor illite formation. The results of this set of experiments indicated that other factors, such as K^+ or Al^{3+} availability, may control illite growth instead of aqueous silica, or that the smectite-to-illite transformation is kinetically limited. However, the experiments conducted in this study utilized a higher water:rock ratio than will likely be observed in the repository-scale environment, which may favor stability of expandable clay minerals (e.g. Whitney 1990). Therefore, these laboratory-scale experiments and findings should be supported by field experiments.

Zeolite Formation

Newly formed zeolite phases with intermediate compositions between analcime ($NaAlSi_2O_6$ (H_2O)) and wairakite ($Ca_{0.5}AlSi_2O_6$ (H_2O)) formed in the 300°C experiments (EBS-14 through EBS-20) but were not identified in the 200°C runs (EBS-21 and EBS-22). Analcime–wairakite formation has been observed in other 200°C experiments, mostly at high pH (Chermak 1992). The absence of analcime–wairakite in the 200°C experiments agrees with previous studies that show analcime crystallization is hindered by high pressure and neutral pH (Wilkin and Barnes 1998; Benning et al. 2000). However, other factors such as the potential for sluggish reaction kinetics, aqueous silica under-saturation, and limited phase stability at lower temperatures should be considered also.

Microprobe analyses of analcime–wairakite show variation in the Si/Al vs. Na/(Na+Ca) for the different experiments from this study and from Cheshire et al. (2013) (Fig. 9). The analcime–wairakite composition range appears to be a result of the bulk composition of the system determining the zeolite-forming reactions, in agreement with Liou et al. (1991) for natural zeolite occurrence in the system $CaAl_2Si_2O_8$–$NaAlSi_3O_8$–SiO_2–H_2O. The low levels of aqueous silica activities and Si/Al ratios observed in this set of experiments may indicate that wairakite is stable with respect to analcime (Liou et al. 1991; Jove-Colon et al. 2016). The crystal structure of the zeolite reaction product is a topic of continued investigation (i.e. orthorhombic analcime vs.

monoclinic wairakite) and the reaction products are referred to as analcime–wairakite.

Newly formed analcime–wairakite grains are observed in two contexts: within the clay matrix and rimming the Opalinus Clay fragments (Fig. 7a–c). The different context of the grains may correspond to different mineral reactions. The compositions of analcime–wairakite within the clay matrix in experiments EBS-15 through EBS-20 have Na/Na+Ca values = 0.52–0.64 and show a relatively flat trend in Si/Al. In comparison, analcime–wairakite grains rimming Opalinus Clay pieces formed in the Opalinus Clay-only experiment (EBS-14) and had the highest Ca content (Na/(Na+Ca) = 0.22) of all experiments (Fig. 9).

In Wyoming bentonite-only systems, previous workers have suggested that analcime formation under similar experimental conditions occurs due to replacement of precursor clinoptilolite dissolution-precipitation (e.g. Chipera and Bish 1997; Wilkin and Barnes 1998; Cheshire et al. 2014) through the reaction:

$$Clinoptilolite + Na^+ \rightarrow Analcime + K^+ + Ca^{2+}$$
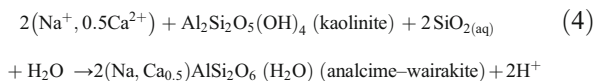$$+ SiO_{2(aq)} + H_2O \quad (3)$$
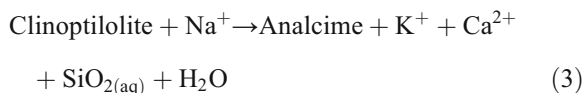
The dissolution of clinoptilolite is interpreted to have contributed to silica saturation with respect to cristobalite in the Wyoming bentonite-only experiments (e.g. EBS-10; Cheshire et al. 2014). The QXRD results from experiments with Wyoming bentonite and Opalinus Clay that formed analcime–wairakite (EBS-15 through EBS-20) indicate the continued presence of clinoptilolite. In some cases (EBS-15, EBS-19), clinoptilolite abundance determined by QXRD increased with respect to an estimate of the starting clinoptilolite abundance. Silica activities remained low (below quartz saturation) in these experiments, which may also indicate that clinoptilolite dissolution was limited and did not occur over the experiment duration.

Unreacted Opalinus Clay does not contain clinoptilolite (Table 3) and, therefore, the analcime–wairakite produced in the Opalinus Clay-only experiment (EBS-14) formed through reactions involving other precursor phases. Analcime–wairakite formation from Ca-rich plagioclase feldspar has been documented (Wirsching 1981); however, albite formed in the experiments (Table 3) and may reflect coupled plagioclase analcime–wairakite solid solution formation as described by Liou et al. (1991). The QXRD results from EBS-14 reveal other significant changes in major-mineral abundances between the starting Opalinus Clay and the reacted sample. Relevant QXRD observations include reduction in kaolinite (17 to 1 wt.%), calcite (16 to 8 wt.%), and quartz (14 to 7 wt.%) (Table 3).

Reactions involving kaolinite and quartz dissolution, as well as feldspar recrystallization, likely provided the aluminum and silica needed for the formation of analcime–wairakite. Levels of aqueous Al^{3+} remained low throughout the experiments, indicating incorporation into silicate-mineral alteration

products. The availability of Na^+ may come from either the synthetic groundwater (Na^+ = 3800 mg/L) or from cation exchange with other clay minerals (e.g. Na-montmorillonite). Calcium was likely derived from calcite and the groundwater (Ca^{2+} = 426 mg/L). The formation of analcime–wairakite from kaolinite has been inferred in high-pH experiments on Opalinus Clay (e.g. Chermak 1992). Analcime–wairakite crystallization from Opalinus Clay materials under the lower-pH conditions of the present experiments likely occurred by the generalized reaction:

$$2(Na^+, 0.5Ca^{2+}) + Al_2Si_2O_5(OH)_4 \text{ (kaolinite)} + 2SiO_{2(aq)} \quad (4)$$

$$+ H_2O \rightarrow 2(Na, Ca_{0.5})AlSi_2O_6 (H_2O) \text{ (analcime–wairakite)} + 2H^+$$

In the Wyoming bentonite and Opalinus Clay experiments, analcime–wairakite crystallization likely occurred during mineral reactions (3) and (4) described above. The larger sodium content observed in the analcime–wairakite in experiments EBS-15 through EBS-20 likely reflects the lower Ca^{2+} availability in the bulk aqueous composition of the system. The formation of analcime–wairakite by reaction (4) may have been the dominant reaction including aqueous silica, thus maintaining the low aqueous silica activities observed throughout the experiment.

These results show that analcime–wairakite formation is a significant mineralogical product both within the bentonite EBS material and along cracks and edges of the argillite wall rock. Further, at high temperatures (i.e. ~300°C) zeolites may form at low pH (4–7). Previous workers have observed abundant analcime formation in the presence of high pH pore fluids (Savage et al. 2007). This study highlights that zeolite formation is also significant within the EBS materials and the host-rock system (i.e. away from the cement liner) at elevated temperatures and pressures.

CONCLUSIONS

The hydrothermal interaction of Wyoming bentonite and Opalinus Clay was tested in an experimental system to gain insight into mineral-brine reactions that may occur in a high-temperature, deep geological nuclear waste repository hosted in argillaceous or clay rock. Experiments conducted at temperatures between 200 and 300°C and water:rock ratios of 6:1 to 9:1 resulted in diverse reaction products, highlighting the influence of temperature, wall-rock, and groundwater geochemistry on the alteration of EBS materials in the near-field environment. Experiments with Opalinus Clay only and brine resulted in clay mineral transformations throughout the Opalinus Clay fragments, but new zeolite formation was observed only along cracks and edges, likely due to the impermeable nature of the argillite as a result of lack of pore space or reactive surfaces. In experiments with both Wyoming bentonite and Opalinus Clay, discrete illite crystallization observed in the experiment run products likely occurred on

precursor illite grains from the Opalinus Clay. Therefore, illitization of the Wyoming bentonite montmorillonite likely did not occur, supporting previous research that emphasizes the effect of bulk composition of the system on clay mineral phase stability. The formation of zeolite minerals with compositions intermediate between those of analcime and wairakite endmembers occurred at low pH through reactions involving precursor zeolite phases or clay minerals. Overall, in the experimental system, zeolite-forming reactions may have controlled the aqueous chemistry, were kinetically favored in comparison to illitization, and may be significant in a high-temperature repository scenario. These experimental results may be used to inform future modeling efforts and full-scale experiments that explore higher thermal loads for disposed spent nuclear fuel and waste than previously considered.

Compliance with Ethical Standards

Conflict of interest
The authors declare that they have no conflict of interest.

REFERENCES

Adler, M., Mäder, U. K., & Waber, H. N. (1999). High-pH alteration of argillaceous rocks: an experimental study. *Schweizerische Mineralogische und Petrographische Mitteilungen, 79*, 445–454.

Benning, L. G., Wilkin, R. T., & Barnes, H. L. (2000). Solubility and stability of zeolites in aqueous solution: II. Calcic clinoptilolite and mordenite. *American Mineralogist, 85*, 495–508. https://doi.org/10.2138/am-2000-0411.

Bish, D. L., & Aronson, J. L. (1993). Paleogeothermal and paleohydrologic conditions in silicic tuff from Yucca Mountain, Nevada. *Clays and Clay Minerals, 41*, 148–161. https://doi.org/10.1346/CCMN.1993.0410204.

Bossart, P.J. & Thury, M. (2008). *Mont Terri Rock Laboratory: Project, Programme 1996 to 2007 and Results*, no. 3. Reports of the Swiss Geological Survey, Wabern.

Bossart, P. & Milnes, A.G. (2017). *Mont Terri Rock Laboratory, 20 Years: Two Decades of Research and Experimentation on*

Claystones for Geological Disposal of Radioactive Waste (Vol. 5): Birkhäuser.

Chermak, J. (1992). Low temperature experimental investigation of the effect of high pH NaOH solutions on the Opalinus Shale, Switzerland. *Clays and Clay Minerals, 40*, 650–658.

Cheshire, M., Caporuscio, F., Jové-Colón, C., & McCarney, M. (2013). Alteration of clinoptilolite into high-silica analcime within a bentonite barrier system under used nuclear fuel repository conditions. *International High–Level Radioactive Waste Management (2013 IHLRWM). Albuquerque, NM.*

Cheshire, M. C., Caporuscio, F. A., Rearick, M. S., Jove-Colon, C., & McCarney, M. K. (2014). Bentonite evolution at elevated pressures and temperatures: An experimental study for generic nuclear repository designs. *American Mineralogist, 99*, 1662–1675. https://doi.org/10.2138/am.2014.4673.

Chipera, S. J., & Bish, D. L. (1997). Equilibrium modeling of clinoptilolite-analcime equilibria at Yucca Mountain, Nevada, USA. *Clays and Clay Minerals, 45*, 226–239. https://doi.org/10.1346/CCMN.1997.0450211.

Chipera, S. J., & Bish, D. L. (2002). FULLPAT: a full-pattern quantitative analysis program for X-ray powder diffraction using measured and calculated patterns. *Journal of Applied Crystallography, 35*, 744–749. https://doi.org/10.1107/S0021889802017405.

Chung, F. H. (1974). Quantitative interpretation of X-ray diffraction patterns of mixtures. I. Matrix-flushing method for quantitative multicomponent analysis. *Journal of Applied Crystallography, 7*, 519–525. https://doi.org/10.1107/S0021889874010375.

Dohrmann, R., & Kaufhold, S. (2014). Cation exchange and mineral reactions observed in MX 80 buffer samples of the Prototype repository in situ experiment in Äspö, Sweden. *Clays and Clay Minerals, 62*, 357–373. https://doi.org/10.1346/CCMN.2014.0620501.

Dohrmann, R., Kaufhold, S., & Lundqvist, B. (2013). The role of clays for safe storage of nuclear waste. Pp. 677–710 in: *Developments in Clay Science* (Vol. 5). Elsevier. doi:https://doi.org/10.1016/B978-0-08-098259-5.00024-X.

Eberl, D., Velde, B., & McCormick, T. (1993). Synthesis of illite-smectite from smectite at earth surface temperatures and high pH. *Clay Minerals, 28*, 49–60. https://doi.org/10.1180/claymin.1993.028.1.06.

Fernández, A. M., Kaufhold, S., Sánchez-Ledesma, D. M., Rey, J. J., Melón, A., Robredo, L. M., Fernández, S., Labajo, M. A., & Clavero, M. A. (2018). Evolution of the THC conditions in the FEBEX in situ test after 18 years of experiment: Smectite crystallochemical modifications after interactions of the bentonite with a C-steel heater at 100°C. *Applied Geochemistry, 98*, 152–171. https://doi.org/10.1016/j.apgeochem.2018.09.008.

Ferrage, E., Vidal, O., Mosser-Ruck, R., Cathelineau, M., & Cuadros, J. (2011). A reinvestigation of smectite illitization in experimental hydrothermal conditions: Results from X-ray diffraction and transmission electron microscopy. *American Mineralogist, 96*, 207–223. https://doi.org/10.2138/am.2011.3587.

Gailhanou, H., Lerouge, C., Debure, M., Gaboreau, S., Gaucher, E. C., Grangeon, S., Grenèche, J. M., Kars, M., Madé, B., Marty, N. C. M., & Warmont, F. (2017). Effects of a thermal perturbation on mineralogy and pore water composition in a clay-rock: an experimental and modeling study. *Geochimica et Cosmochimica Acta, 197*, 193–214. https://doi.org/10.1016/j.gca.2016.10.004.

Greenberg, H., Wen, J., & Buscheck, T. (2013). Scoping Thermal Analysis of Alternative Dual-Purpose Canister Disposal Concepts. Lawrence Livermore National Laboratory. LLNL-TR-639869.

Guillaume, D., Neaman, A., Cathelineau, M., Mosser-Ruck, R., Peiffert, C., & Abdelmoula, M. (2003). Experimental synthesis of chlorite from smectite at 300°C in the presence of metallic Fe. *Clay Minerals, 38*, 281–302. https://doi.org/10.1180/0009855033830096.

Hadi, J., Wersin, P., & Serneels, V. (2019). Eighteen years of steel–bentonite interaction in the FEBEX in situ test at the Grimsel Test Site in Switzerland. *Clays and Clay Minerals, 67*, 111. https://doi.org/10.1007/s42860-019-00012-5.

Heimann, R. B. (1993). Brønsted acidification observed during hydrothermal treatment of a calcium montmorillonite. *Clays and Clay Minerals, 41*, 718–725. https://doi.org/10.1346/CCMN.1993.0410610.

Hofmann, H., Bauer, A., & Warr, L. N. (2004). Behavior of smectite in strong salt brines under conditions relevant to the disposal of low-to medium-grade nuclear waste. *Clays and Clay Minerals, 52*, 14–24. https://doi.org/10.1346/CCMN.2004.0520102.

Honty, M., Wang, L., Osacký, M., Uhlík, P., Czímerová, A., & Madejová, J. (2012). Experimental interactions of the Opalinus Clay and Boom Clay with various repository relevant solutions at 90 C under closed conditions. *Applied Clay Science, 59*, 50–63. https://doi.org/10.1016/j.clay.2012.02.011.

Johannesson, L. E., Börgesson, L., Goudarzi, R., Sandén, T., Gunnarsson, D., & Svemar, C. (2007). Prototype repository: A full scale experiment at Äspö HRL. *Physics and Chemistry of the Earth, Parts A/B/C, 32*, 58–76. https://doi.org/10.1016/j.pce.2006.04.027.

Johnston, R.M. & Miller, H.G. (1984). *The effect of pH on the stability of smectite* (No. AECL–8366). Atomic Energy of Canada Ltd..

Jove-Colon, C.F., Hammond, G.E., Kuhlman, K.L., Zheng, L., Kim, K., & Xu, H. (2016). Evaluation of used fuel disposition in clay-bearing rock. Sandia National Laboratories (SNL-NM).

Kasbohm, J., Herbert, H. J., & Henning, K. H. (2005). Short- and long term stability of selected bentonites in high saline solutions, International Symposium on Large-scale Fields in Granite, Sitges, Barcelona, Spain, November 12–14, 2003. *Code, 88404*, 231–240.

Kaufhold, S., & Dohrmann, R. (2010). Stability of bentonites in salt solutions: II. Potassium chloride solution—Initial step of illitization? *Applied Clay Science, 49*, 98–107. https://doi.org/10.1016/j.clay.2010.04.009.

Kaufhold, S., & Dohrmann, R. (2009). Stability of bentonites in salt solutions | sodium chloride. *Applied Clay Science, 45*, 171–177. https://doi.org/10.1016/j.clay.2009.04.011.

Leupin, O. X., Birgersson, M., Karnland, O., Korkeakoski, P., Mäderm, U. K., Sellin, P., & Wersin, P. (2014). Montmorillonite stability under nearfield conditions. *Nagra Tech. Rep. NTB*, 14–12.

Liou, J. G., de Capitani, C., & Frey, M. (1991). Zeolite equilibria in the system CaAl$_2$Si$_2$O$_8$–NaAlSi$_3$O$_8$–SiO$_2$–H$_2$O. *New Zealand Journal of Geology and Geophysics, 34*, 293–301. https://doi.org/10.1080/00288306.1991.9514467.

Madsen, F. (1998). Clay mineralogical investigations related to nuclear waste disposal. *Clay Minerals, 33*, 109–129. https://doi.org/10.1180/000985598545318.

Martin, P. L., Barcala, J. M., & Huertas, F. (2006). Large-scale and long-term coupled thermo-hydro-mechanic experiments with bentonite: the FEBEX mock-up test. *Journal of Iberian Geology, 32*, 259–282.

Meunier, A., Velde, B., & Griffault, L. (1998). The reactivity of bentonites: a review. An application to clay barrier stability for nuclear waste storage. *Clay Minerals, 33*, 187–196. https://doi.org/10.1180/000985598545462.

Moore, D. M., & Reynolds, R. C. (1997). *X-ray Diffraction and the Identification and Analysis of Clay Minerals.* Oxford, UK: Oxford University Press.

Mosser-Ruck, R., Cathelineau, M., Baronnet, A., & Trouiller, A. (1999). Hydrothermal reactivity of K-smectite at 300°C and 100 bar: dissolution-crystallization process and non-expandable dehydrated smectite formation. *Clay Minerals, 34*, 275–290.

Mosser-Ruck, R., Cathelineau, M., Guillaume, D., Charpentier, D., Rousset, D., & Barres, O. (2010). Effects of temperature, pH, and iron/clay and liquid/clay ratios on experimental conversion of dioctahedral smectite to berthierine, chlorite, vermiculite, or saponite. *Clays and Clay Minerals, 58*, 280–291. https://doi.org/10.1346/CCMN.2010.0580212.

Mosser-Ruck, R., Pignatelli, I., Bourdelle, F., Abdelmoula, M., Barres, O., & Guillaume, D. (2016). Contribution of long-term hydrothermal experiments for understanding the smectite-to-chlorite conversion in geological environments. *Contributions to Mineralogy and Petrology, 171*. https://doi.org/10.1007/s00410-016-1307-z.

Müller, H.R. et al. (2018) Implementation of the full-scale emplacement (FE) experiment at the Mont Terri rock laboratory. In: *Mont Terri Rock Laboratory, 20 Years* (P. Bossart and A. Milnes, editors). Swiss Journal of Geosciences Supplement, vol 5. Birkhäuser, Cham. https://doi.org/10.1007/978-3-319-70458-6_15

NAGRA (2002). *Project Opalinus Clay: safety report: demonstration of disposal feasibility for spent fuel, vitrified high-level waste and long-lived intermediate-level waste (Entsorgungsnachweis)*: Nagra.

Neuhoff, P. S., & Ruhl, L. S. (2006). Mechanisms and geochemical significance of Si–Al substitution in zeolite solid solutions. *Chemical Geology, 225*, 373–387. https://doi.org/10.1016/j.chemgeo.2005.08.029.

Pearson, F. (2002). Benken reference water chemistry. *Unpubl. Nagra Int. Report. Nagra, Wettingen, Switzerland*.

Pearson, F., Arcos, D., Boisson, J., Fernandez, A., Gäbler, H., & Gaucher, E. (2003). Mont Terri project—Geochemistry of water in the Opalinus clay formation at the Mont Terri Rock Laboratory. Synthesis Report. Geol. Rep. no. 5. Swiss National Hydrological and Geological Survey, Ittigen-Bern, Switzerland. *Mont Terri project—Geochemistry of water in the Opalinus clay formation at the Mont Terri Rock Laboratory. Synthesis Report. Geol. Rep. no. 5. Swiss National Hydrological and Geological Survey, Ittigen-Bern, Switzerland.*, -.

Pouchou, J. & Pichoir, F. (1984). PAP correction procedure for improved quantitative microanalysis. (pp. 104–106): San Francisco Press San Francisco, CA.

Pusch, R. (2001). The microstructure of MX-80 clay with respect to its bulk physical properties under different environmental conditions. Swedish Nuclear Fuel and Waste Management Co.

Pusch, R. (1979). Highly compacted sodium bentonite for isolating rock-deposited radioactive waste products. *Nuclear Technology, 45*, 153–157.

Pusch, R. & Kasbohm, J. (2002). Alteration of MX-80 by hydrothermal treatment under high salt content conditions. Swedish Nuclear Fuel and Waste Management Co.

Pusch, R., & Madsen, F. T. (1995). Aspects on the illitization of the Kinnekulle bentonites. *Clays and Clay Minerals, 43*, 261–270. https://doi.org/10.1346/CCMN.1995.0430301.

Pusch, R., Takase, H., & Benbow, S. (1998). Chemical processes causing cementation in heat-affected smectite-the Kinnekulle bentonite. Swedish Nuclear Fuel and Waste Management Co.

Rimstidt, J. D., & Barnes, H. L. (1980). The kinetics of silica-water reactions. *Geochimica et Cosmochimica Acta, 44*, 1683–1699. https://doi.org/10.1016/0016-7037(80)90220-3.

Savage, D., Walker, C., Arthur, R., Rochelle, C., Oda, C., & Takase, H. (2007). Alteration of bentonite by hyperalkaline fluids: A review of the role of secondary minerals. *Physics and Chemistry of the Earth, Parts A/B/C, 32*, 287–297. https://doi.org/10.1016/j.pce.2005.08.048.

Savage, D., Wilson, J., Benbow, S., Sasamoto, H., Oda, C., & Walker, C. (2019). Natural systems evidence for the effects of temperature and the activity of aqueous silica upon montmorillonite stability in clay barriers for the disposal of radioactive wastes. *Applied Clay Science, 179*, 105146. https://doi.org/10.1016/j.clay.2019.105146.

Sellin, P., & Leupin, O. (2014). The use of clay as an engineered barrier in radioactive waste management – a review. *Clays and Clay Minerals, 61*, 477–498. https://doi.org/10.1346/CCMN.2013.0610601.

Seyfried Jr, W. (1987). Rocking autoclaves for hydrothermal experiments. II. The flexible reaction-cell system. *Hydrothermal Experimental Techniques*, 216–239.

Smyth, J. (1982). Zeolite stability constraints on radioactive waste isolation in zeolite-bearing volcanic rocks. *The Journal of Geology, 90*, 195–202.

Taubald, H., Bauer, A., Schäfer, T., Geckeis, H., Satir, M., & Kim, J. (2000). Experimental investigation of the effect of high-pH solutions on the Opalinus Shale and the Hammerschmiede Smectite. *Clay Minerals, 35*, 515–524. https://doi.org/10.1180/000985500546981.

Wersin, P., Johnson, L. H., & McKinley, I. G. (2007). Performance of the bentonite barrier at temperatures beyond 100°C: A critical review. *Physics and Chemistry of the Earth, Parts A/B/C, 32*, 780–788. https://doi.org/10.1016/j.pce.2006.02.051.

Wieczorek, K., Gaus, I., Mayor, J. C., Schuster, K., García-Siñeriz, J.-L., & Sakaki, T. (2017). In-situ experiments on bentonite-based buffer and sealing materials at the Mont Terri rock laboratory (Switzerland). *Swiss Journal of Geoscience., 110*, 253–268. https://doi.org/10.1007/s00015-016-0247-y.

Wilkin, R., & Barnes, H. (1998). Solubility and stability of zeolites in aqueous solution: I. Analcime, Na-, and K-clinoptilolite. *American Mineralogist, 83*, 746–761. https://doi.org/10.2138/am-1998-7-807.

Wirsching, U. (1981). Experiments on the hydrothermal formation of calcium zeolites. *Clays and Clay Minerals, 29*, 171–183. https://doi.org/10.1346/CCMN.1981.0290302.

Whitney, G. (1990). Role of water in the smectite-to-illite reaction. *Clays and Clay Minerals, 38*, 343–350.

Wolery, T.J. & Jarek, R.L. (2003). EQ3/6, Version 8.0: Software User's Manual. Albuquerque, Sandia National Laboratories: 376 pp.

Wolery, T.J. & Jové Colón, C.F. (2007). Qualification of Thermodynamic Data for Geochemical Modeling of Mineral–Water Interactions in Dilute Systems (ANL-WIS-GS-000003 REV 01). Las Vegas, Nevada, Sandia National Laboratories; OCRWM Lead Laboratory for Repository Systems: 412 pp.

Zheng, L., Rutqvist, J., Birkholzer, J. T., & Liu, H. H. (2015). On the impact of temperatures up to 200 C in clay repositories with bentonite engineer barrier systems: A study with coupled thermal, hydrological, chemical, and mechanical modeling. *Engineering Geology, 197*, 278–295. https://doi.org/10.1016/j.enggeo.2015.08.026.